

RESEARCH ARTICLE

OPEN ACCESS



Guizhi-Shaoyao-Zhimu decoction attenuates bone erosion in rats that have collagen-induced arthritis via modulating NF-κB signalling to suppress osteoclastogenesis

Shu-jun Wei^a , Qing Zhang^b, Yong-jing Xiang^a, Lan-yu Peng^c, Wei Peng^b, Qiang Ren^c and Yong-xiang Gao^a

^aSchool of Basic Medicine, Chengdu University of Traditional Chinese Medicine, Chengdu, China; ^bSchool of Pharmacy, Chengdu University of Traditional Chinese Medicine, Chengdu, China; ^cHospital of Chengdu, University of Traditional Chinese Medicine, Chengdu, China

ABSTRACT

Context: *Guizhi-Shaoyao-Zhimu* decoction (GSZD) is commonly used to treat rheumatoid arthritis (RA), but its mechanism is unclear.

Objective: To investigate the effect of GSZD on bone erosion in type II collagen (CII)-induced arthritis (CIA) in rats and to identify the underlying mechanism.

Materials and methods: The CIA model was prepared in male Wistar rats by two subcutaneous injections of CII, 1 mg/mL. Fifty CIA rats were randomized equally into the control group given saline daily, the positive group given saline daily and methotrexate 0.75 mg/kg once a week, and three GSZD-treated groups gavaged daily with 800, 1600 and 3200 mg/kg of GSZD for 21 days. GSZD effects were assessed by paw volume, arthritic severity index and histopathology. Cytokine levels were determined by ELISA. The effects of GSZD on RAW264.7 cells were evaluated by receptor activator of NF-κB ligand (RANKL)-induced osteoclastogenesis and bone resorption assay. Expression of IκB-α and p65 was measured by Western blotting. Major components of GSZD were identified by HPLC.

Results: Arthritis index score, paw volume and bone destruction score showed that GSZD improved inflammatory symptoms and reduced joint tissue erosion ($p < 0.01$). GSZD decreased RANKL, and the number of osteoclasts (OCs) in joint tissues ($p < 0.01$) and increased osteoprotegerin levels ($p < 0.01$). GSZD inhibited RANKL-induced RAW264.7 differentiation and reduced bone resorption by OCs. GSZD upregulated IκB ($p < 0.01$) and p65 ($p < 0.01$) in the cytoplasm and downregulated p65 ($p < 0.01$) in the cell nucleus.

Conclusions: *Guizhi-Shaoyao-Zhimu* decoction has an anti-RA effect, suggesting its possible use as a supplement and alternative drug therapy for RA.

ARTICLE HISTORY

Received 29 April 2020

Revised 12 December 2020

Accepted 9 January 2021

KEYWORDS

Rheumatoid arthritis;
osteoclast; RANKL;
osteoprotegerin

Introduction

Rheumatoid arthritis (RA) is a common autoimmune disease that causes systemic inflammation and recurrent disease of the joints. Globally, RA affects 0.5–1.0% of people (Scott et al. 2010; Cross et al. 2014; Sparks 2019). RA manifests in humans primarily as joint pain, swelling and deformity, but this condition also affects several organs such as the lung, cardiovascular system, skin and others. The most prominent feature of RA is symmetrical pain and swelling of the hands, wrists, feet and knees, known as polyarthritis, although other joints may also be affected (Aletaha and Smolen 2018). Recent studies have shown that the pathological changes of RA include chronic synovial inflammation, proliferation of synovial cells, synovial angiogenesis, pannus formation and damage to cartilage and bone (Scott et al. 2010; Sparks 2019). During the early stage of the pathogenesis of RA, bone damage is manifested as loss of bone mass around joints, and in the late stages as subchondral bone destruction and systemic osteoporosis (OP) (Sinigaglia et al. 2006; Jin et al. 2018).

Normal bone maintenance is the result balancing the formation of bone promoted by osteoblasts (OBs) with the resorption of bone by osteoclasts (OCs). In RA patients, bone metabolism is characterized by increased bone destruction and insufficient bone formation, and this imbalance is recognized as the primary cause of systemic OP and local joint bone destruction (Sinigaglia et al. 2006; Walsh and Gravallese 2010; Jin et al. 2018). OCs mediate bone destruction by intercellular interaction and regulation of various cytokines, which is the main cause of joint damage in RA (Fardellone et al. 2014). OCs are multi-karyocytes derived from the fusion of haematopoietic stem cell precursors in the bone marrow. OC precursors (OCPs) enter the circulating blood following their activation by chemokines (Chambers 2000). When the OCPs arrive at the segment of bone undergoing absorption, also known as the bone remodelling unit (BRU), they may enter the bone tissue and differentiate into OCs under the control of a series of chemokines and cytokines. Two key factors expressed by BRU and its surrounding cells are receptor activator of NF-κB ligand (RANKL) and macrophage

CONTACT Wei Peng  pengwei@cdutcm.edu.cn  School of Pharmacy, Chengdu University of Traditional Chinese Medicine, No. 1166 Liu-tai Road, Chengdu 611130, China; Qiang Ren  401627406@qq.com  Hospital of Chengdu, University of Traditional Chinese Medicine, No. 39 Shi-er-qiao Road, Chengdu 610072, China; Yong-xiang Gao  drgaoxy@cdutcm.edu.cn  International Education College, Chengdu University of Traditional Chinese Medicine, 37 Shi-er-qiao Rd., Jinniu District, Chengdu 610075, China

colony-stimulating factor (M-CSF). These cytokines promote generalized or local bone absorption during normal or pathological bone remodelling by regulating the formation and differentiation of OCPs (Chambers 2000; Boyce 2013). RANKL binds to RANK, leading to TRAF6 adaptor protein recruitment, followed by NF- κ B activation which is essential for osteoclastogenesis and bone absorption, and its activation primarily depends on the phosphorylation of the I κ B α inhibitory subunit and nuclear translocation of p65. RANKL and osteoprotegerin (OPG) have a critical function in the maintenance of the dynamic balance between bone creation and resorption. The RANK/RANKL complex is activated following the induction of several cytokines including M-CSF, interleukin (IL)-1, IL-6, IL-8, tumour necrosis factor (TNF)- α and IL-17 (Simonet et al. 1997; Gravallese 2003; Vanderborgh et al. 2004; Kim et al. 2009; Redlich and Smolen 2012). After the binding of RANKL to RANK, the receptor of OCP is formed, next inducing the activation and differentiation of OCs. On this basis, previous research suggested that the levels of RANKL/RANK/OPG can be used as a key indicator of the degree of OC-mediated bone resorption (Xu et al. 2012; Walsh and Choi 2014; Brzustewicz and Bryl 2015; Papadaki et al. 2019).

Guizhi-Shaoyao-Zhimu decoction (GSZD), a well-known Chinese medicine formula, was first recorded in the Synopsis of Prescriptions of the Golden Chamber. GSZD is composed of the twigs of *Cinnamomum cassia* (L.) J. Presl (Lauraceae), the radix of *Cynanchum otophyllum* CK Schneid (Paeoniaceae), the rhizome of *Anemarrhena asphodeloides* Bunge (Liliaceae), the radix and rhizome of *Glycyrrhiza uralensis* Fisch. ex DC. (Leguminosae), the whole plant of *Ephedra sinica* Stapf (Ephedraceae), the rhizome of *Zingiber officinale* Roscoe (Zingiberaceae), the rhizome of *Atractylodes macrocephala* Koidz (Asteraceae), the radix of *Saposhnikovia divaricata* (Turcz.) Schischk. (Umbelliferae) and the processed lateralis radix of *Aconitum carmichaelii* Debeaux (Ranunculaceae). The GSZD has been widely applied to treat arthritis and its related diseases for more than 1000 years. Clinical studies have demonstrated that GSZD can reduce inflammatory responses, suppress immunity, improve microcirculation and reduce joint swelling and pain. Due to these properties, this decoction has been used clinically as a reliable alternative and complementary approach to treating RA (Guo et al. 2016; Daily et al. 2017). However, the mechanistic basis for the beneficial effects of GSZD in the treatment of RA remains to be identified. As such, herein we sought to determine the anti-bone destruction properties of GSZD in rats with type II collagen-induced arthritis (CIA) and the effect of GSZD on the induction of OCs by RANKL, and to identify the potential mechanisms responsible for the activity of the decoction. The obtained information would be beneficial for the expansion GSZD clinical utility.

Materials and methods

Herbal components of in GSZD and preparation of GSZD extracts

Neautus Chinese Herbal Pieces Ltd. Co. (Chengdu, China) was the source of all herbal drugs, and their identity was verified by Prof. Chun-Jie Wu (School of Pharmacy, Chengdu University of Traditional Chinese Medicine, Chengdu, China). The voucher specimens of the herbal drugs were deposited at the Herbarium of Laboratory (the twigs of *C. cassia* (no. 20180407GZD-1), the radix of *C. otophyllum* (no. 20180407GZD-2), the rhizome of *A. asphodeloides* (no. 20180407GZD-3), the radix and rhizome

of *G. uralensis* (no. 20180407GZD-4), the whole plant of *E. sinica* (no. 20180407GZD-5), the rhizome of *Z. officinale* (no. 20180407GZD-6), the rhizome of *A. macrocephala* (no. 20180407GZD-7), the radix of *S. divaricata* (no. 20180407GZD-8) and the processed lateralis radix of *A. carmichaelii* (no. 20180407GZD-9)). All drugs were soaked 10 times in pure water for 30 min and then concentrated under vacuum at 60 °C. The water extracts of GSZD were freeze-dried and preserved in a dry environment.

Drugs and reagents

Complete and incomplete Freund's adjuvant (CFA and IFA), and methotrexate (MTX) were purchased from Sigma-Aldrich Chemical Co. (St. Louis, MO). Bovine type II collagen (CII) was provided by Chondrex Inc. (Seattle, WA). Rat TNF- α , IL-1 β , IL-6, IL-8, IL-17A, M-CSF, RANKL and OPG ELISA kits, radioimmuno-precipitation assay (RIPA) lysis buffer and phenylmethane-sulfonyl fluoride (PMSF) were obtained from Elabscience Biotech Co. (Wuhan, China). Haematoxylin-eosin (H&E) staining kit, Modified Safranine O-Fast Green (SFG) FCF Cartilage staining kit, 1% toluidine blue and 2.5% glutaraldehyde were purchased from Solarbio Biotech Co. (Beijing, China). A TRAP stain kit was from Multisciences Biotech Co. (Hangzhou, China). The α modification of Eagle's minimum essential medium (α -MEM), Dulbecco's modified Eagle's medium (DMEM), foetal bovine serum (FBS), were from Gibco-BRL (Sydney, Australia). Bovine serum albumin (BSA) was from BioFROXX (Berlin, Germany). RANKL was from PeproTech (Rocky Hill, NJ). Specific primary antibodies against p65, I κ B, histone H3 and GAPDH, as well as the secondary antibody, goat anti-rabbit IgG (H + L)-HRP, were obtained from Affinity Biosciences, Inc. (Cincinnati, OH). A CCK-8 kit was from the Elabscience Biotech Co. (Wuhan, China). The National Institutes for Food and Drug Control (Beijing, China) was the source of all other compounds.

Animals

Male Wistar rats (6–7 weeks of age) from Chengdu Dashuo Biotechnology Co. (Chengdu, China) were caged in a standard facility (12 h light/dark cycle; 20–24 °C) with free food and water access. Animals were given a 1-week acclimatization period prior to experimentation. The Laboratory Animal Research Centre of Chengdu University of Traditional Chinese Medicine approved all studies, which conformed to the Regulations for Laboratory Animal Management.

CIA model

CIA was induced in rats by injecting with CII using a previously described protocol with minor modifications (Brand et al. 2007; Dekkers et al. 2017). CII was dissolved in 0.05 M acetic acid (at 2 mg/mL) and emulsified using CFA or IFA at a 1:1 ratio (final concentration: 1 mg/mL CII). CFA was used to prepare this solution for the initial day 0 injection, whereas IFA was used for the second injection on day 14. For the first injection, subcutaneous injections of 0.3 mL of the emulsion were administered into the left and right sides of the back of each rat and at the tail base. For the second injection, a total of 0.2 mL of the emulsion was subcutaneously injected into one point at the back and the tail base, for a total of two points. Normal saline (NS) was administered to controls.

Experimental protocols

The rats were separated into six groups ($n=10$): the normal group, control group, positive group and different doses of GSZD groups. The experimental procedure is shown in Figure 1(A). Rats were selected on 21 days after initial injection. A total of CIA 50 rats were successfully prepared, and 21 days after initial injection, the animals were randomly divided into five groups. The four groups rats were treated orally for three weeks with MTX (positive control drug, 0.75 mg/kg/week) or GSZD (800, 1600 and 3200 mg/kg/d). Control and normal group rats were given NS (10 mL/kg) orally. During the treatment period, the determinations of paw volume and arthritis index score were performed every three days. On the 20th day, three rats in each group were selected for micro-computed tomography (micro-CT) imaging of the knee and ankle joints. After 21 days of the treatment, rats were anaesthetized using sodium pentobarbital (40 mg/kg, ip) and blood samples were collected from the abdominal aorta. Subsequently, the animals were sacrificed and the ankle joints and synovial tissue of knee joints were collected for further analysis.

Arthritis score assessment

A standard scoring system (0–4) was used to assess the severity of the arthritis in the hind paw of each rat, as follows: 0 = no evidence of swelling or redness; 1 = swelling of the ginger joints in a given paw; 2 = mild swelling in the wrist or ankle joint of a given paw; 3 = severely inflamed paw; 4 = paw is deformed or exhibits ankyloses. Both hind paws were scored for each rat, and

were added together to yield polyarthritic index values (0–8). Two researchers independently evaluated each rat every third day during treatment.

Paw volume measurement

The paw volume of each group of rats was measured utilizing a paw volume metre. A mark was made on the bony process of the heel of the affected side of the rat, and the hind paw of the rat was dipped into the measuring cup so that the mark was level with the water line and the volume of the displaced water was recorded. During the experiment, the same hind paw was selected for each measurement. The measurements were performed every three days in all rats.

Micro-CT imaging of knee and ankle joints

Micro-CT imaging was performed at the Core Facility of West China Hospital (Chengdu, China) on day 20. Plain and 3D reconstruction images of the affected knee and ankle joints were obtained in rats anaesthetized using sodium pentobarbital (40 mg/kg, ip). Scanning parameters were as follows: 90 kV, 80 mA, FOV: 72, voxel size: 45–90, scan mode: high resolution and scan time: 4 min. Bone destruction in the knee and ankle joints was scored as 0, 1, 2 or 3 (no, minor, moderate or severe damage). The final bone destruction score was the sum of scores for the two joints (0–6).

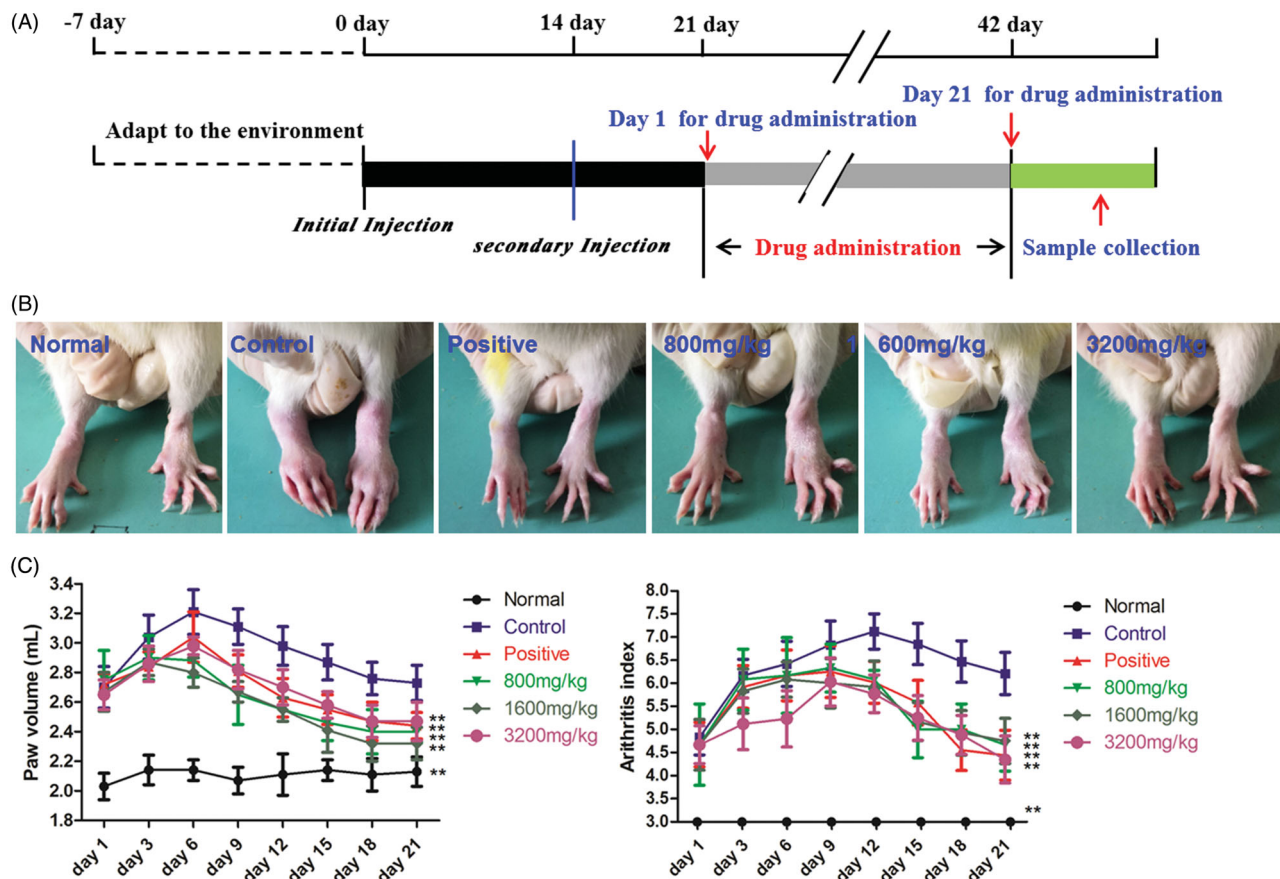


Figure 1. Anti-arthritis activities of GSZD. (A) Overview of methods. (B) Representative images of the joints of CIA rats in different groups. (C) GSZD impact on the changes in paw volume (left) and arthritis score (right) in CIA rats.

Histopathology

After rats were euthanized, ankle joints of the rats were separated, fixed using 10% paraformaldehyde (PFA), decalcified, and embedded in paraffin via a standard approach paraffin-embedded using standard histologic techniques. Serial sections were H&E and SFG stained to assess morphology of bone and cartilage. To identify and analyse OCs, the remaining ankle joints were stained by TRAP staining which was performed according to the manufacturers' instructions.

Cytokine and protease level measurements

Serum samples were separated from whole blood using high-speed centrifugation ($2000 \times g$, 15 min, 4°C). Supernatants were collected and frozen at -80°C . TNF- α , IL-1 β , IL-6, IL-8, IL-17A, M-CSF, RANKL and OPG levels were quantified based on instructions from commercial ELISA kits. Synovial tissue of the knee joint was treated with lysis buffer (RIPA:PMSF = 100:1) using 100 μL of the buffer per 10 mg of synovial tissue. The samples were fully homogenized (velocity: 4.0 m/s, time: 90 s), centrifuged at $2000 \times g$ for 10 min at 4°C , and the supernatants were used for the determination of the concentration of RANKL and OPG by ELISA.

Cell culture

RAW264.7 cells from Beina Biological Company (Beijing, China) were grown in DMEM containing 10% FBS and penicillin in a humidified 37°C incubator containing 5% CO₂. DMSO was used to dissolve GSZD which was diluted in DMEM to achieve the final concentration of DMSO of less than 0.1% (v/v).

Cell viability assay

How GSZD affected RAW264.7 viability was assessed via CCK-8 assay. Cells were plated on 96-well plates with 3×10^4 cells per well. Different concentrations of GSZD (100, 200, 400, 800, 1600, 3200, 6400, 12,800 and 25,600 $\mu\text{g}/\text{mL}$) were added and incubated for 24, 48 and 72 h. At the end of incubation, 10 μL of the reaction liquid was added to each well, and incubated for 2 h at 37°C . Viability was analysed with a Bio-Rad iMark microplate reader (Hercules, CA) using the absorbance at 450 nm.

Osteoclastogenesis and TRAP staining

RAW264.7 cells were plated in 24-well plates ($1 \times 10^4/\text{well}$) in complete α -MEM containing 80 ng/mL RANKL and GSZD (0, 200, 400 and 800 $\mu\text{g}/\text{mL}$). Untreated cells served as a negative control, while RANKL alone was used for treating positive controls. The culture medium was changed every other day. Following a seven-day culture, PBS was used to wash cells which were then fixed with 4% PFA for 20 min, and stained to detect TRAP activity. Multinuclear TRAP-positive cells were enumerated via microscope. The number of mature OCs with more than three nuclei was counted in a random area in each of the replicate samples.

Bone resorption assay

RAW264.7 cells added to 96-well plates (1×10^4 per well) containing bovine bone slices. To these cells was added α -MEM and

treated with RANKL (80 ng/mL) and different concentrations of GSZD (200, 400 and 800 $\mu\text{g}/\text{mL}$). After nine days, the cells were washed using PBS, fixed in 2.5% glutaraldehyde over 7 min, washed with 0.25 mol/L ammonia hydroxide with ultrasonic cleaning, and stained for 10 min with 1% toluidine blue. After washing in ddH₂O, the formation of osteolysis pits was observed and photographed under a light microscope. Bone resorption capacity was expressed as the relative area of bone resorption (resorption area/total bone area).

Western blotting

RAW264.7 cells were added at $2 \times 10^6/\text{well}$ in plates for 24 h. Cells were pre-treated for 3 h with GSZD (0, 200, 400 and 800 $\mu\text{g}/\text{mL}$) and then induced for 30 min by RANKL (80 ng/mL) with equivalent GSZD concentrations. Ice-cold RIPA buffer was used for total protein extraction. Nuclear (N) or cytoplasmic (C) proteins were isolated with the cytoplasmic and nuclear proteins extraction kits, and protein concentrations were determined via BCA assay. Equal amounts of proteins were separated via SDS-PAGE prior to PVDF membrane transfer. Blots were blocked for 1 h with TBST containing 5% BSA, followed by overnight incubation at 4°C with primary antibodies. Next, membranes were washed and probed using species-matched HRP-conjugated secondary antibody for 1 h. An ECL imaging system was used to visualize protein, with Image J (v1.51, National Institutes of Health, Bethesda, MD) being used to visualize protein bands.

HPLC assessment of the main constituents in GSZD extracts

The main chemical constituents in GSZD were identified by HPLC extracts. Chromatographic separation was performed using the Shimadzu LC-2030C3 D High-Performance Liquid Chromatograph (Tokyo, Japan). The sample was separated with a Phenomenex 100A C₁₈ column (250 mm \times 4.6 mm, 5 μm) at 32°C using a gradient elution at a flow rate of 0.8 mL/min. We used 0.1% formic acid–water (A) and 1% formic acid–acetonitrile (B) as the mobile phase. A gradient program was set as: 0–5 min, 1% B; 5–10 min, 1–2% B; 20–25 min, 2–10% B; 25–35 min, 10% B; 35–40 min, 10–12% B; 40–45 min, 12% B; 45–55 min, 12–18% B; 55–60 min, 18–20% B; 60–70 min, 20–30% B; 70–95 min, 30–45% B; and 95–105 min, 45% B. The volume of injected sample was 10 μL and the detection wavelength was set at 254 nm.

Statistical analysis

All values are means \pm SD. SPSS (v22.0, SPSS Inc., Chicago, IL) was used for statistical testing, and significance was determined by one-way analysis of variance (ANOVA) with the LSD test. $p < 0.05$ was the significance threshold.

Results

GSZD improves joints symptoms in CIA rats

How GSZD affected CIA symptoms in rats was examined first. Swelling of the ankle joint is the first CIA clinical sign in rats. The performance of the ankle joint in each group of rats after 21 days of the treatment is illustrated in Figure 1(B). In comparison with normal controls, the ankle joint of the control CIA rats showed evident swelling; however, the swelling was alleviated by MTX and GSZD. Furthermore, the effects of MTX and GSZD

on the arthritis score and paw volume in rats were evaluated from the first day of drug administration to the end of the experiment. As shown in Figure 1(C), the paw volume and arthritic scores of control rats were higher than in normal rats at each time point ($p < 0.01$). Importantly, the treatment with MTX (0.75 mg/kg/week) and GSZD (800, 1600 and 3200 mg/kg/d) significantly decreased the arthritis score and paw volume of CIA rats ($p < 0.01$) at most of the time points.

GSZD attenuates bone erosion of joints in CIA rats

Synovial inflammation and joint and cartilage damage in ankle joints were examined histologically using H&E stained tissue sections. CIA rats exhibited obvious bone erosion, joint cavity

stenosis, synovial hyperplasia and inflammatory cell infiltration (Figure 2). However, in a manner comparable to MTX, treatment of CIA rats with GSZD (800, 1600 and 3200 mg/kg/d) markedly attenuated the bone erosion of joints in CIA rats and preserved nearly normal morphology of ankle joints with a smooth cartilage surface, reduced evidence of infiltration by mononuclear cells, as well as decreased synovial hyperplasia. A safranin O-fast green staining approach also revealed that GSZD and MTX suppressed ankle cartilage damage in these rats (Figure 3).

Micro-CT imaging (Figure 4) documented that, in comparison with the normal rats, the inner malleolus and outer ankle joint surfaces of the control rats were not uniform, the joint space was narrow, the joint surface was fused and the joint structure was seriously damaged ($p < 0.01$). Varying degrees of bone

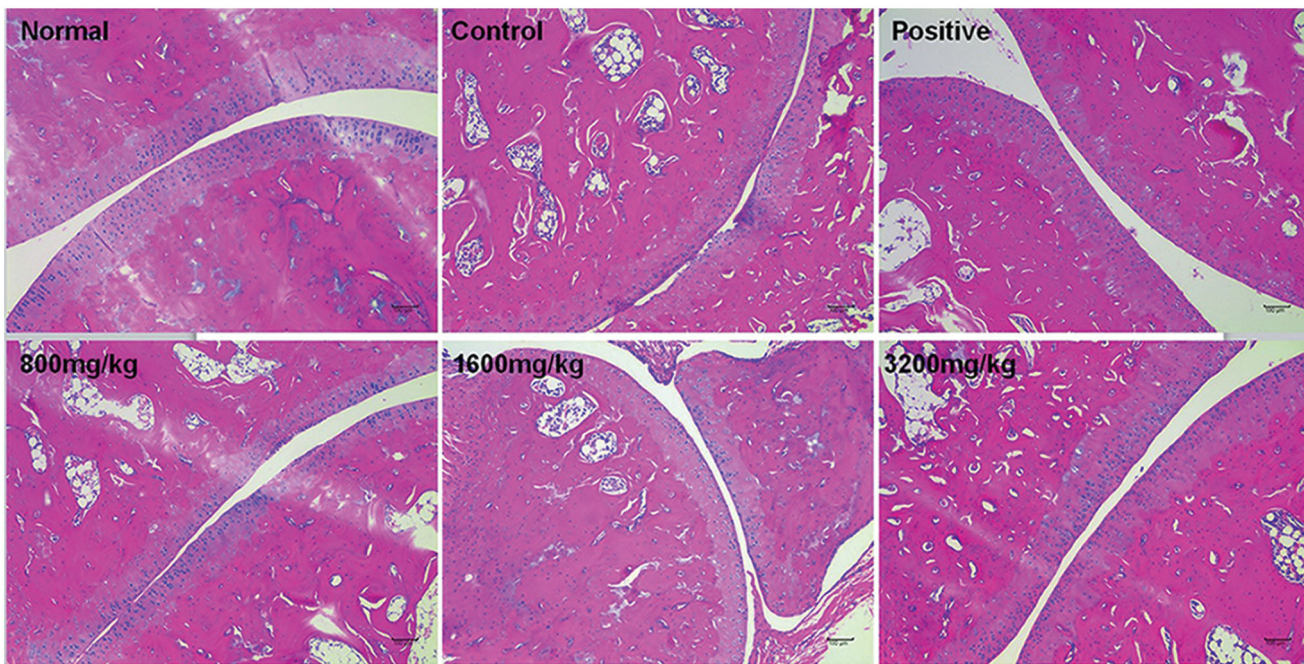


Figure 2. GSZD impact on ankle joint histopathology in CIA model rats visualized by the H&E staining.

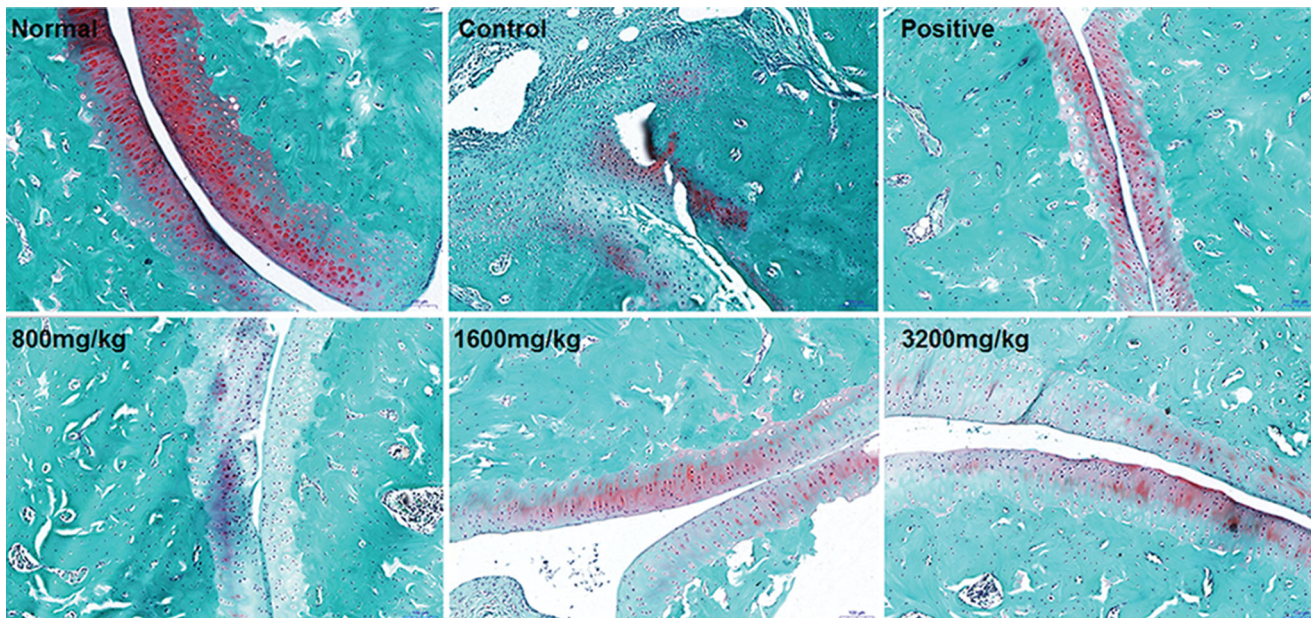


Figure 3. GSZD impact on ankle joint histopathology in CIA model rats visualized by the safranin O-fast green staining.

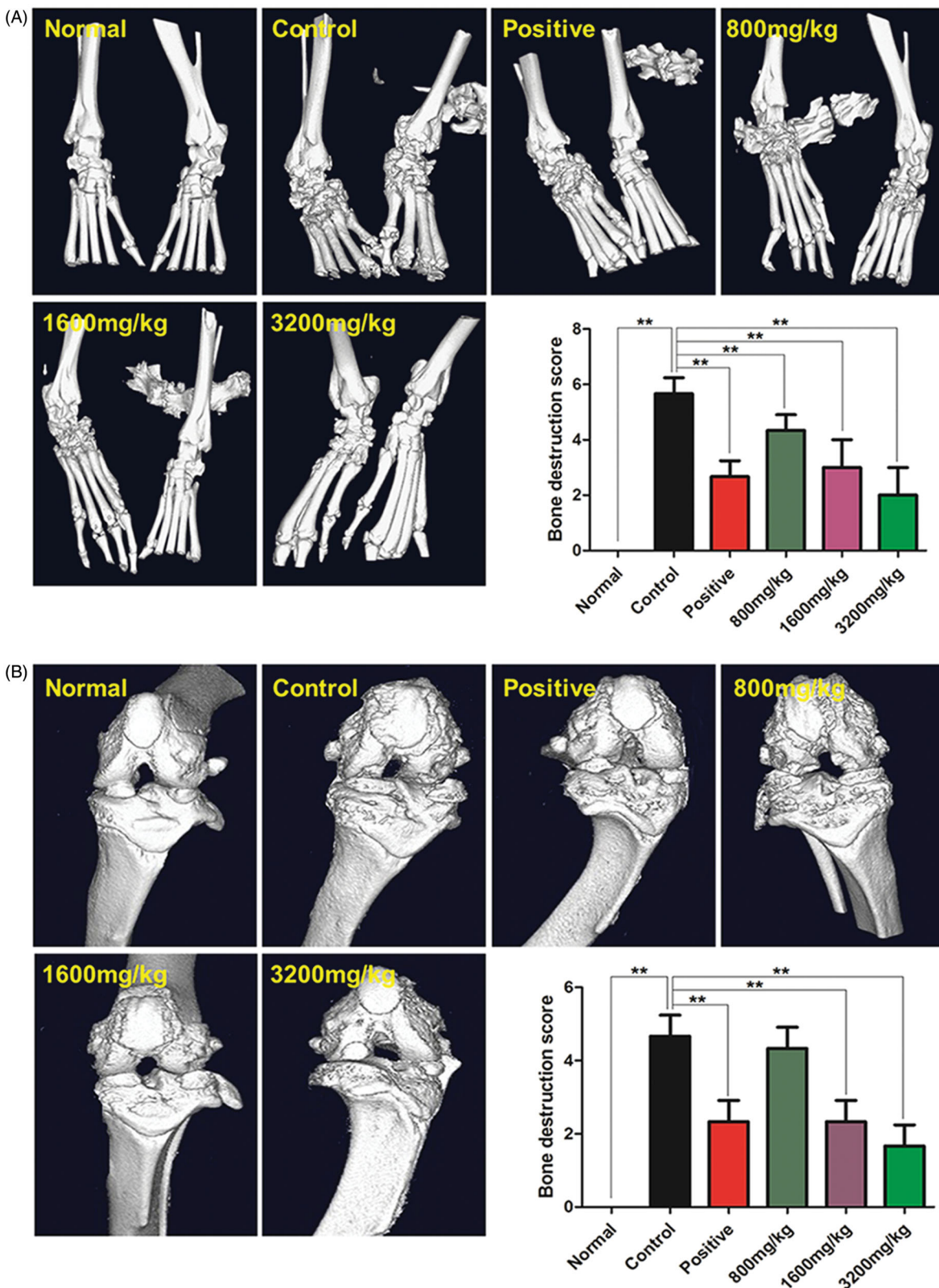


Figure 4. Results of the micro-CT imaging of ankle joints (A) and knee joints (B) of CIA rats. Data are the mean \pm SD ($n = 6$), ** $p < 0.01$ vs. control.

of ankle joint injury were detected in all treatment groups, but MTX and GSZD reduced the damage of ankle bone relative to the control group ($p < 0.01$). Moreover, the knee joint of the rats in the normal group exhibited no bone damage, and the joint structure was clear. In contrast, the joint surface of the lower femoral border and the upper tibial border in control rats was

rough with bone erosion-like changes, and the joint space was evidently narrow ($p < 0.01$, Figure 4(B)). The treatment with MTX and GSZD reduced the destruction of the knee joint versus control rats ($p < 0.01$). These findings suggest that GSZD protects joints and cartilage from damage and deformity in CIA rats.

GSZD decreases the osteoclasts in ankle joints of CIA rats

TRAP is a characteristic marker enzyme of OCs, and its detection is often used to determine the number, volume and functional status of OCs (Tsuboi et al. 2003). TRAP staining demonstrated that the number of OCs in control rats was significantly higher than in normal rats (Figure 5). Relative to control rats, the number of OCs decreased after the administration of MTX or GSZD, indicating that GSZD suppresses the proliferation of OCs in joints tissues of CIA rats.

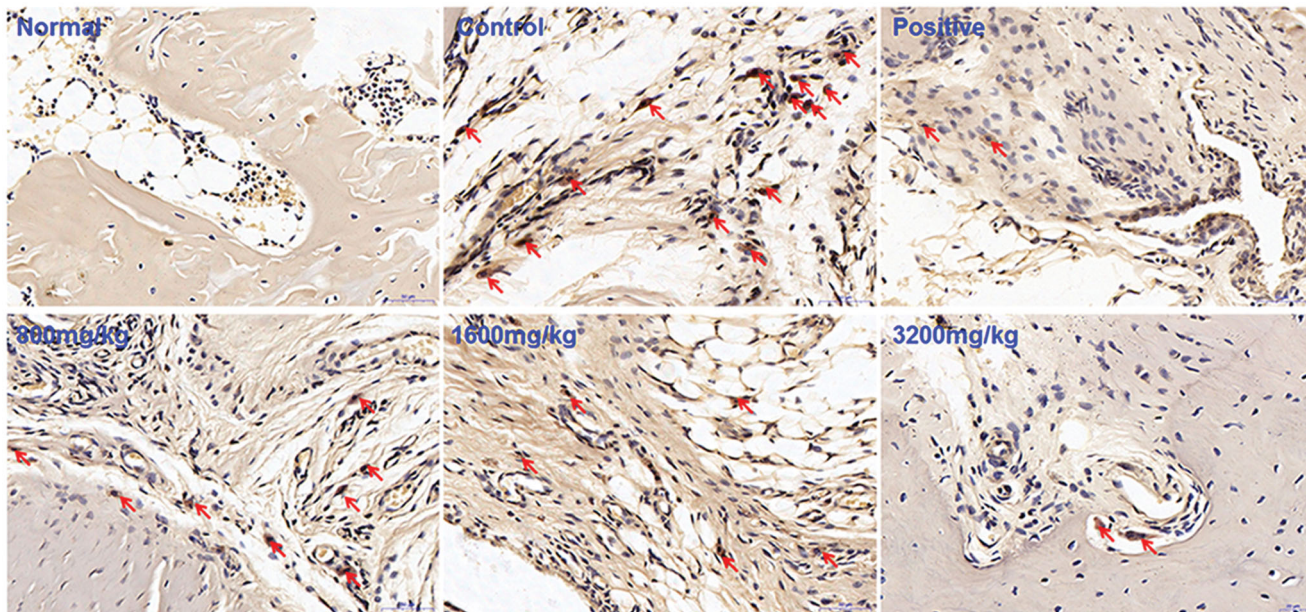


Figure 5. Effects of GSZD on the changes in osteoclasts of the ankle joint of CIA rats detected by TRAP staining (arrows indicate osteoclasts).

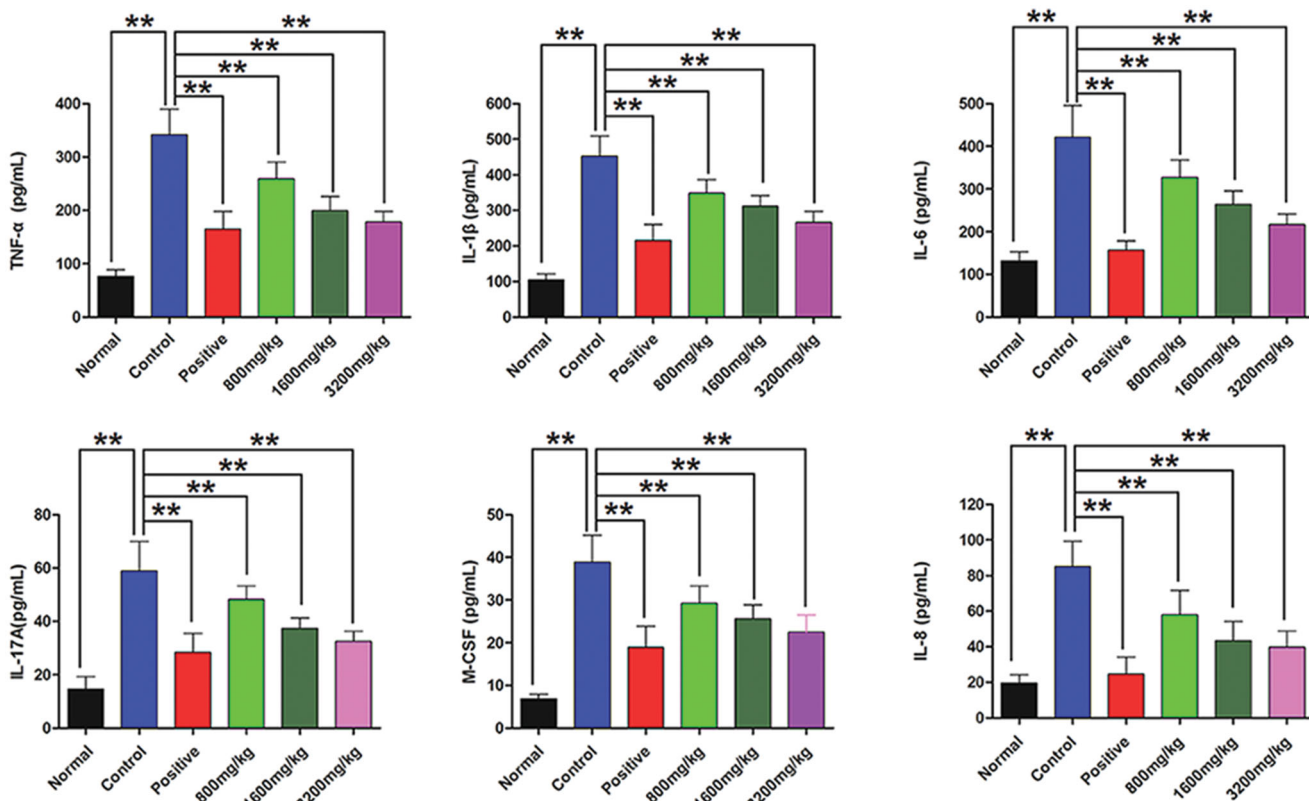


Figure 6. Effects of GSZD on serum levels of pro-inflammatory cytokines. Data are presented as the mean \pm SD ($n = 10$), ** $p < 0.01$ vs. control rats.

GSZD decreases circulating pro-inflammatory cytokine levels

To determine the possible mechanisms responsible for the protective effect of GSZD on CIA rat joints, the impact of GSZD on serum concentrations of damage-related pro-inflammatory mediators was determined. Serum TNF- α , IL-1 β , IL-6, IL-17A, IL-8 and M-CSF levels in the control group were markedly elevated relative to those in normal controls ($p < 0.01$, Figure 6). Of relevance, treatment with GSZD and MTX decreased serum pro-inflammatory cytokine levels ($p < 0.01$, vs. control rats).

GSZD regulates the expression of RANKL and OPG in CIA rats

Figure 7(A,B) summarizes the results of the measurements of the level of RANKL and OPG in serum and synovial tissues. The concentration of RANKL in serum and synovial tissues was significantly higher in control than in normal rats ($p < 0.01$), while the levels of OPG were markedly decreased ($p < 0.01$). The treatment with GSZD or MTX significantly reduced RANKL ($p < 0.01$) and increased OPG ($p < 0.01$) levels in both serum and synovial tissues of CIA rats.

GSZD inhibits osteoclastogenesis and bone resorption in RANKL-stimulated RAW264.7 cells

GSZD cytotoxicity on RAW264.7 cells was assessed via CCK-8 assays. As shown in Figure 8, GSZD at concentrations up to 0.8 mg/mL did not exhibit significant toxicity against RAW264.7 cells at all time points. The concentration- and time-dependent effect of GSZD on osteoclastogenesis was examined next.

At seven days after the stimulation of RAW264.7 cells by RANKL, TRAP-positive multinucleated cells were formed (Figure 9(A)). Interestingly, GSZD at 200, 400 and 800 μ g/mL markedly reduced the number of OCs in a dose-dependent fashion ($p < 0.05$ at 200 μ g/mL, $p < 0.01$ at 400 and 800 μ g/mL). Additionally, the effects of GSZD on *in vitro* bone resorption were determined. In comparison with the control group, bone

resorption pits were markedly decreased by GSZD in a dose-dependent fashion ($p < 0.01$, Figure 9(B)).

GSZD inhibits NF- κ B signalling

Western blotting documented that the RAW264.7 cells stimulated by RANKL significantly decreased the level of I κ B α ($p < 0.01$) and p65 ($p < 0.01$) in the cytoplasm and increased the

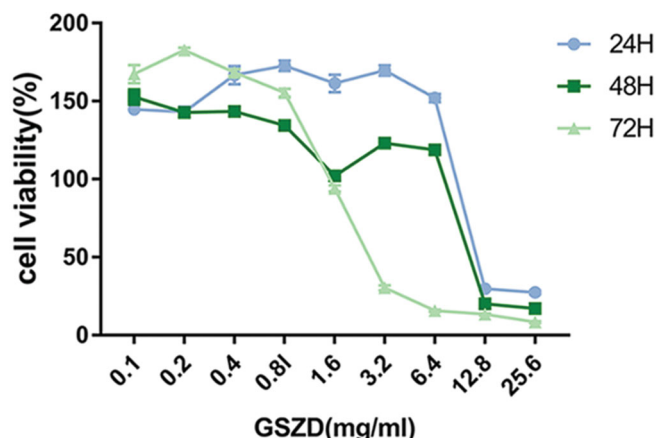


Figure 8. Cytotoxic effect of GSZD on RAW264.7 cells determined by the CCK-8 assay.

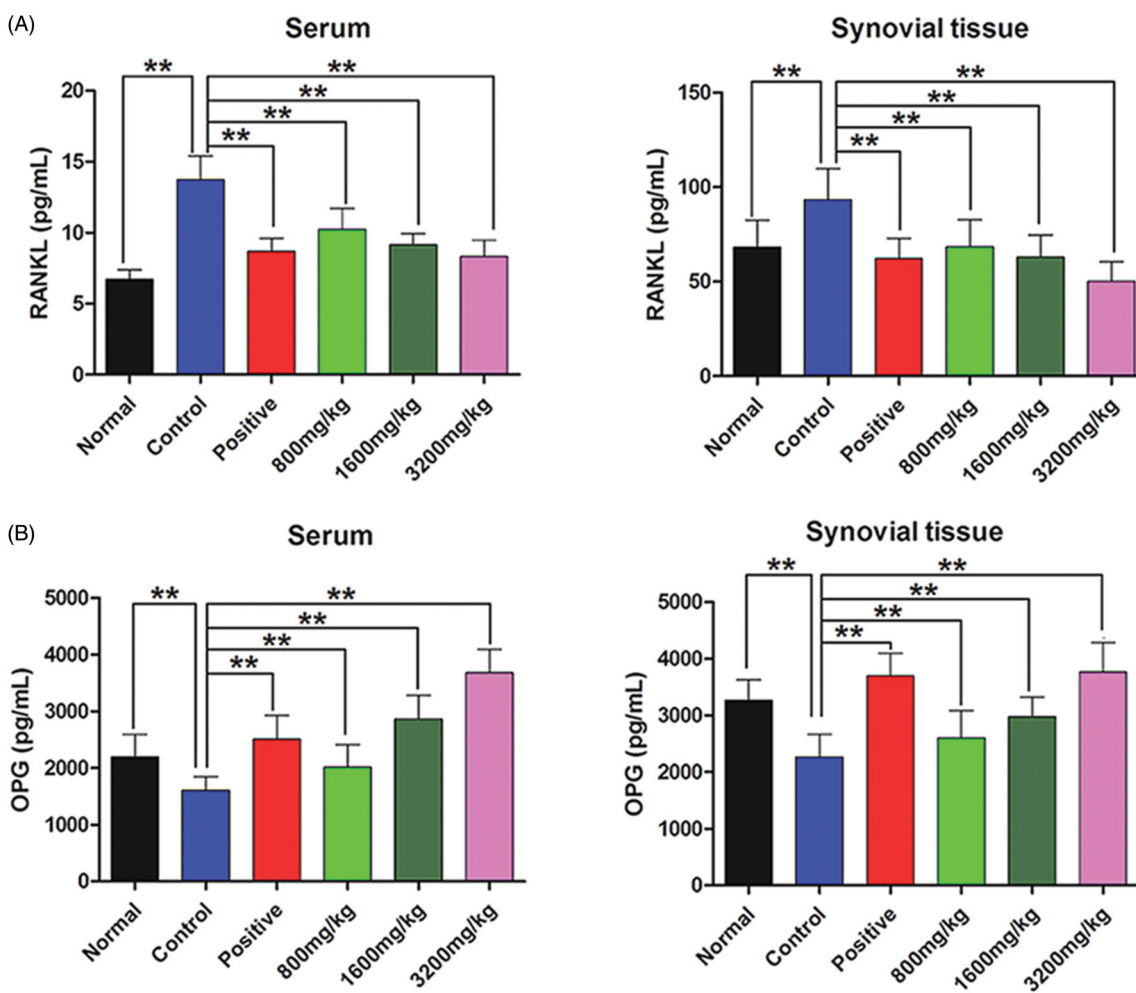


Figure 7. Effects of GSZD on the expression of RANKL (A) and OPG (B) in serum and synovial tissues. Data are the mean \pm SD ($n = 10$), ** $p < 0.01$ vs. control.

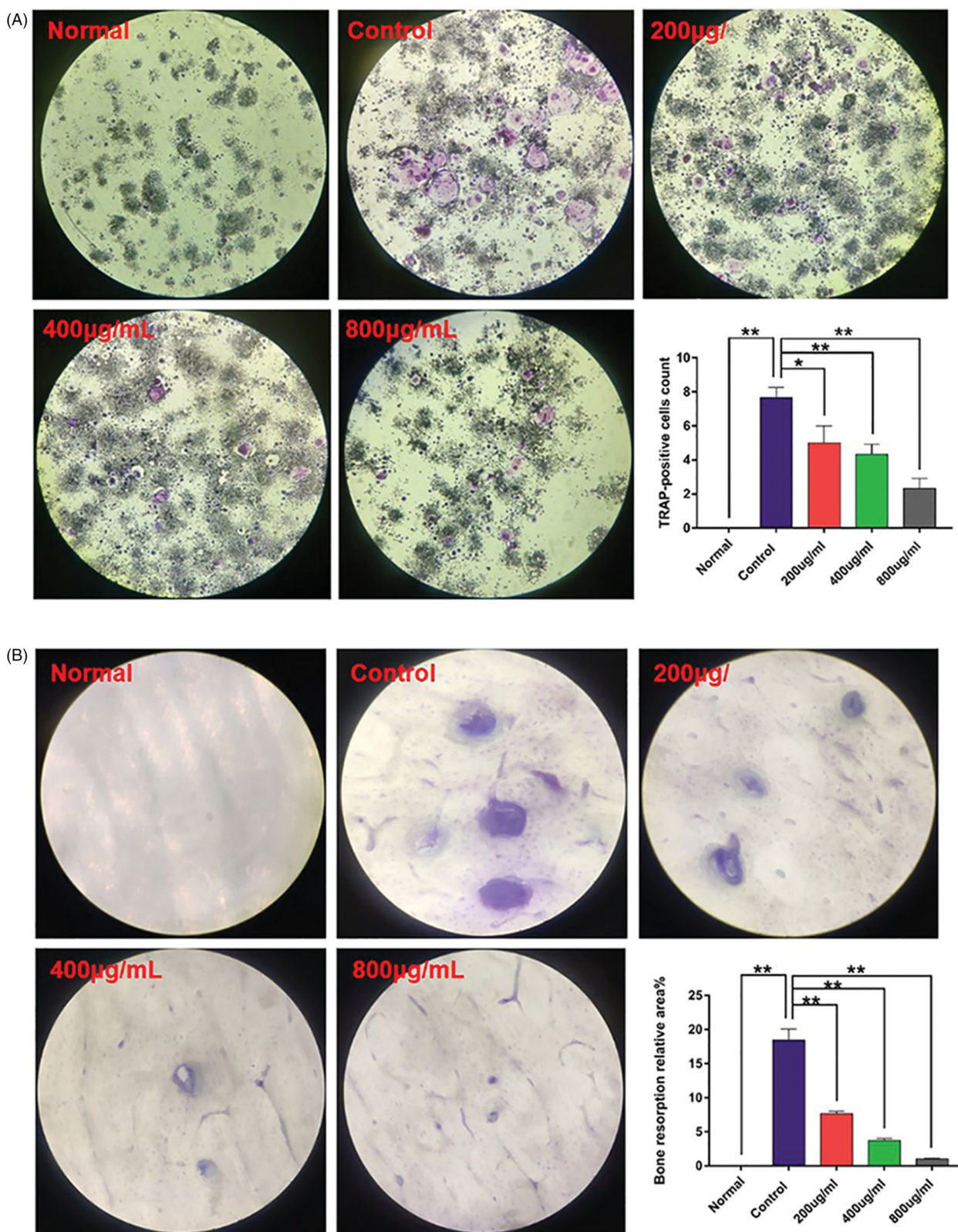


Figure 9. Effects of GSZD on TRAP staining (A) and bone resorption assay (B). Data are presented as the mean \pm SD ($n = 3$), * $p < 0.05$, ** $p < 0.01$ vs. control.

level of p65 in the nucleus ($p < 0.01$, Figure 10). Exposure of cells to GSZD at 200, 400 and 800 $\mu\text{g}/\text{mL}$ markedly upregulated expression of I κ B α ($p < 0.01$) and p65 ($p < 0.01$) in the cytoplasm while decreasing p65 level in the nucleus ($p < 0.01$). These results indicate that GSZD suppresses the RANKL-induced activation of the NF- κ B signalling pathway.

HPLC analysis

Findings from an HPLC-based assessment of the chemical composition of GSZD are listed in Figure 11. By comparison with the reference data (Qin et al. 2019) and standards agents, six main chemical compounds were identified in GSZD extracts:

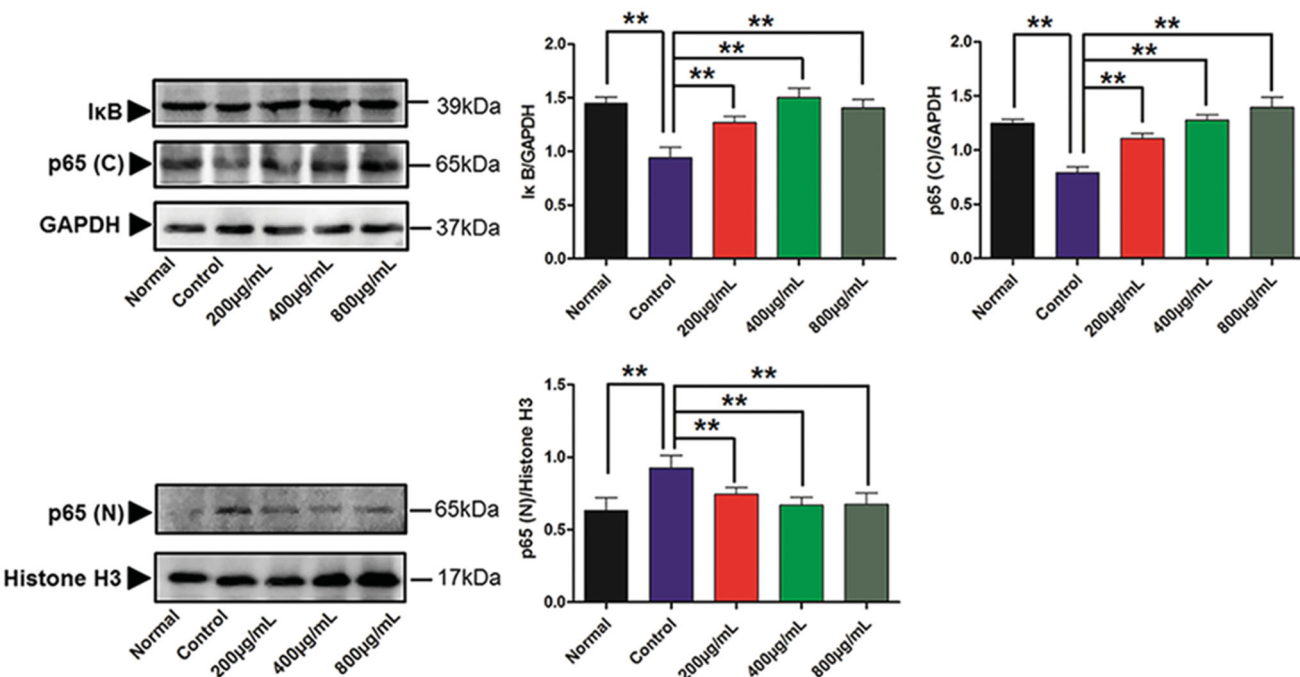


Figure 10. Effects of GSZD on the activation of the NF-κB signalling pathway in RANKL-induced OCs. Data are presented as mean \pm SD ($n=3$), ** $p < 0.01$ vs. control.

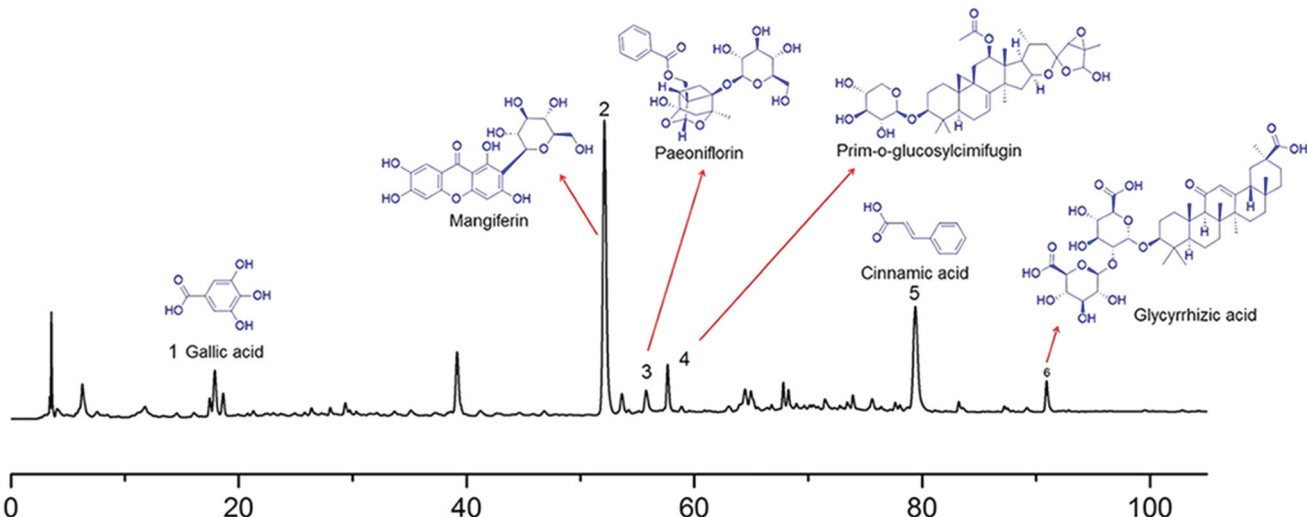


Figure 11. HPLC analysis of the composition of GSZD. Numbers 1–6 represent gallic acid, mangiferin, paeoniflorin, prim-O-glucosylcimifugin, cinnamic acid and glycyrrhizic acid, respectively.

gallic acid, mangiferin, paeoniflorin, prim-O-glucosylcimifugin, cinnamic acid and glycyrrhizic acid.

Discussion

Currently, five categories of RA pharmaceutical agents, which include non-steroidal anti-inflammatory drugs (NSAIDs), glucocorticoids, DMARDs and small molecule-targeted DMARDs, biosimilars and botanical drug preparations, are commonly used for treating RA clinically (Scott et al. 2010; Chingcuanco et al. 2016; Singh et al. 2016; Smolen et al. 2017; Aletaha and Smolen 2018; Bridges et al. 2018). However, these drugs could produce serious adverse effects such as infection, kidney injury, anaemia and liver function abnormalities. Moreover, the cost of these medications and their limited effectiveness in some patients are driving the

need to develop new drugs, particularly small molecules, or natural products. With the progress in traditional Chinese medicine, some of its preparations exhibiting an anti-RA activity are gradually approved for clinical use. The natural products approved for clinical use contain various compounds such as *Tripterygium* glycosides, total glucosides of paeony and sinomenine have definite curative effects in treating RA (Chen et al. 2013; Yang et al. 2013; Jia et al. 2014; Xiang et al. 2015; Liu et al. 2018; Wang et al. 2018; Huang et al. 2019). As one of the famous prescriptions of traditional Chinese medicine, GSZD is successfully used to treat RA, osteoarthritis and OP. In the present investigation, a rat model of CIA has been employed to investigate the potential of GSZD in RA therapy and reveal the mechanism of its anti-RA activity.

To reach these objectives, a CIA rat model was successfully generated. The experiments demonstrated the GSZD has a

beneficial effect against joint damage in CIA. In this experiment, the experimental doses of GSZD were based on the clinical commonly used doses for human (93 g/60 kg/d, crude herb medicine equivalent). This dose of GSZD for human transferred to rats are approximately 9.3 g/kg/d (crude herb medicine equivalent). In addition, the water extraction yields of GSZD is approximately 18%, and therefore the dose for rats regarding water extracts of GSZD are approximately 1600 mg/kg. Consequently, in our present study, we selected the 1600 mg/kg as the middle dose, and 800 and 3200 mg/kg/day as the low and high doses. After 21 days of treatment of CIA rats with GSZD, their arthritis index and paw volume were significantly reduced. Histopathologic examination based on H&E and SFG documented that GSZD reduced bone and cartilage damage, decreased local infiltration by inflammatory cells, and inhibited synovial hyperplasia and pannus formation. Micro-CT imaging demonstrated that GSZD inhibited the progression of joint injury in CIA rats. Importantly, joint damage in CIA rats visualized by CT imaging closely resembles that seen in human RA. The pathogenesis of joint damage involves the proliferation of the synovium that can invade the cartilage and subchondral bone, and with numerous OCs that have been activated being present at the junction between the pannus and the bone. In those with RA, joint destruction can result from bone resorption driven by OCs from the proliferating synovium (Gravallese et al. 2000; Atkins et al. 2006). Therefore, the number of ankle OCs in CIA rats was evaluated using the TRAP staining. Interestingly, GSZD inhibited the proliferation of OCs in joints of CIA rats.

The differentiation and maturation of OCs are regulated by many factors, but the key mechanism controlling these processes involves the interaction among OPG, RANKL and RANK. Immune cells involved in RA pathogenesis can directly upregulate RANKL, or indirectly increase its expression via the secretion of pro-inflammatory cytokines, promoting the formation, differentiation and activation of OC (Brennan and McInnes 2008; McInnes et al. 2016). Previous studies have shown that these functions are mediated by M-CSF, TNF- α , IL-1 β , IL-6,

IL-8 and IL-17A (Nakae et al. 2003; Adamopoulos et al. 2010; Edwards and Weivoda 2012; Komatsu and Takayanagi 2015). The results of the current work show that GSZD can reduce the level of pro-inflammatory cytokines. Our *in vivo* work raised the possibility that the bone-protective effect of GSZD might be associated with the downregulation of M-CSF, TNF- α , IL-1 β , IL-6, IL-8 and IL-17A and consequent suppression of expression of RANKL and upregulation of OPG.

To explore in greater detail the mechanisms of GSZD activity against bone destruction, the effects of GSZD on RANKL-induced OCs were investigated using RAW264.7 cells. Upon stimulation by RANKL, these cells generate bone-resorbing multinucleated OCs and, therefore, are widely used in studies of OCs differentiation. Based on cell viability analysis and preliminary experiments (Zhang et al. 2019), we chose 200, 400 and 800 μ g/mL as the experimental doses of GSZD *in vitro*. The ability of RAW264.7 cells to differentiate into OCs after activation by RANKL was confirmed in the current investigation, and the cells were used to determine whether GSZD can inhibit the formation of OCs by RANKL-stimulated cells and bone resorption. The obtained results showed that GSZD markedly suppressed both processes. The early activation of RANKL-responsive signalling pathways is critical for the efficient induction of OC formation. In RAW264.7 cells, one of the earliest and most important of these pathways is the NF- κ B signalling cascade (Wu et al. 2012). Therefore, we have advanced the hypothesis that GSZD may inhibit OCs formation and specific protein expression by affecting the NF- κ B signalling pathway. It has also been shown that the NF- κ B signalling pathway has an essential function in osteoclastogenesis by stimulating the commitment of OCPs to the OC lineage and promoting their maturation. NF- κ B pathway activation depends primarily on the phosphorylation of I κ B α and p65 nuclear translocation. RANKL induces CRel and NF- κ B1 (p50) binding to DNA, as well as the formation of RelA (p65) NF- κ B complexes via the NF- κ B pathway (Figure 12). The present work demonstrated that the treatment of cells with GSZD suppresses the RANKL-induced NF- κ B activation by

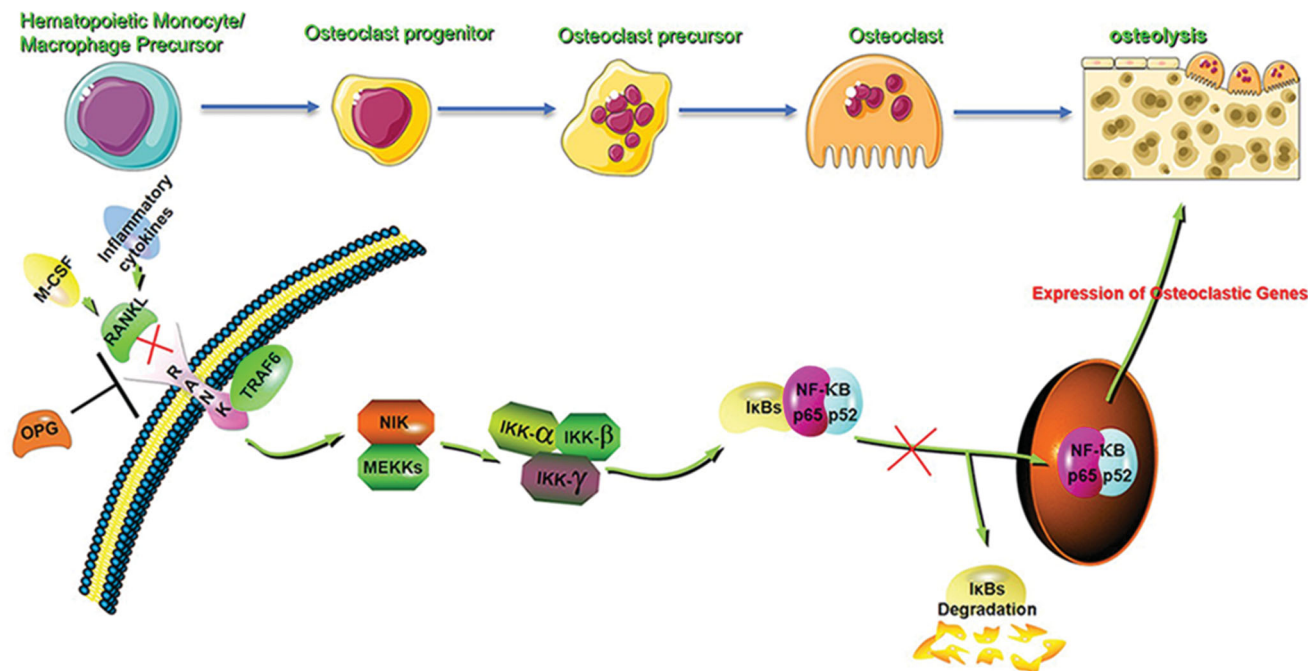


Figure 12. The mechanism of attenuation of RANKL-induced bone resorption by GSZD. GSZD suppresses the activation of NF- κ B signalling during the differentiation of OCs.

suppressing the degradation of I κ B α and attenuates the nuclear translocation and transcriptional activity of p65.

Conclusions

The results of this study suggest that GSZD attenuates bone erosion in collagen-induced arthritis in rats by suppressing osteoclastogenesis via the regulation of NF- κ B signalling. This work will help to identify the pharmacological mechanism of anti-RA activity of GSZD and provide a reference for future complementary and alternative medicine therapies for RA.

Disclosure statement

The authors declare that there are no conflicts of interest.

Funding

This work was supported by the National Science and Technology Major Project of the Ministry of Science and Technology of China [No. 2018ZX09721004-009-002], Sichuan Science and Technology Program [No. 2019JDRCC0074] and Xinglin Scholar Discipline Promotion Talent Program of Chengdu University of Traditional Chinese Medicine [No. BSH2018006].

ORCID

Shu-jun Wei  <http://orcid.org/0000-0002-2343-8107>

References

- Adamopoulos IE, Chao CC, Geissler R, Laface D, Blumenschein W, Iwakura Y, McClanahan T, Bowman EP. 2010. Interleukin-17A upregulates receptor activator of NF- κ B on osteoclast precursors. *Arthritis Res Ther*. 12(1):R29.
- Aletaha D, Smolen JS. 2018. Diagnosis and management of rheumatoid arthritis: a review. *JAMA*. 320(13):1360–1372.
- Atkins G, Kostakis P, Vincent C, Farrugia AN, Houchins JP, Findlay DM, Evdokiou A, Zannettino AC. 2006. RANK expression as a cell surface marker of human osteoclast precursors in peripheral blood, bone marrow, and giant cell tumors of bone. *J Bone Miner Res*. 21(9):1339–1349.
- Boyce BF. 2013. Advances in the regulation of osteoclasts and osteoclast functions. *J Dent Res*. 92(10):860–867.
- Brand DD, Latham KA, Rosloniec EF. 2007. Collagen-induced arthritis. *Nat Protoc*. 2(5):1269–1275.
- Brennan FM, McInnes IB. 2008. Evidence that cytokines play a role in rheumatoid arthritis. *J Clin Invest*. 118(11):3537–3545.
- Bridges SL Jr, White DW, Worthing AB, Gravallese EM, O'Dell JR, Nola K, Kay J, Cohen SB. 2018. The science behind biosimilars: entering a new era of biologic therapy. *Arthritis Rheumatol*. 70(3):334–344.
- Brzustewicz E, Bryl E. 2015. The role of cytokines in the pathogenesis of rheumatoid arthritis—practical and potential application of cytokines as biomarkers and targets of personalized therapy. *Cytokine*. 76(2):527–536.
- Chambers TJ. 2000. Regulation of the differentiation and function of osteoclasts. *J Pathol*. 192(1):4–13.
- Chen Z, Li XP, Li ZJ, Xu L, Li XM. 2013. Reduced hepatotoxicity by total glucosides of paeony in combination treatment with leflunomide and methotrexate for patients with active rheumatoid arthritis. *Int Immunopharmacol*. 15(3):474–477.
- Chingcuanco F, Segal JB, Kim SC, Alexander GC. 2016. Bioequivalence of biosimilar tumor necrosis factor- α inhibitors compared with their reference biologics: a systematic review. *Ann Intern Med*. 165(8):565–574.
- Cross M, Smith E, Hoy D, Carmona L, Wolfe F, Vos T, Williams B, Gabriel S, Lassere M, Johns N, et al. 2014. The global burden of rheumatoid arthritis: estimates from the global burden of disease 2010 study. *Ann Rheum Dis*. 73(7):1316–1322.
- Daily JW, Zhang T, Cao S, Park S. 2017. Efficacy and safety of GuiZhi-ShaoYao-ZhiMu decoction for treating rheumatoid arthritis: a systematic review and meta-analysis of randomized clinical trials. *J Altern Complement Med*. 23(10):756–770.
- Dekkers JS, Schoones JW, Huizinga TW, van der Helm-van Mil AH. 2017. Possibilities for preventive treatment in rheumatoid arthritis? Lessons from experimental animal models of arthritis: a systematic literature review and meta-analysis. *Ann Rheum Dis*. 76(2):458–467.
- Edwards JR, Weivoda MM. 2012. Osteoclasts: malefactors of disease and targets for treatment. *Discov Med*. 13(70):201–210.
- Fardellone P, Sejourne A, Pacco J, Goeb V. 2014. Bone remodelling markers in rheumatoid arthritis. *Mediators Inflamm*. 2014:484280.
- Gravallese EM. 2003. Osteopontin: a bridge between bone and the immune system. *J Clin Invest*. 112(2):147–149.
- Gravallese EM, Manning C, Tsay A, Naito A, Pan C, Amento E, Goldring SR. 2000. Synovial tissue in rheumatoid arthritis is a source of osteoclast differentiation factor. *Arthritis Rheum*. 43(2):250–258.
- Guo Q, Mao X, Zhang Y, Meng S, Xi Y, Ding Y, Zhang X, Dai Y, Liu X, Wang C, et al. 2016. Guizhi-Shaoyao-Zhimu decoction attenuates rheumatoid arthritis partially by reversing inflammation-immune system imbalance. *J Transl Med*. 14(1):165–165.
- Huang RY, Pan HD, Wu JQ, Zhou H, Li ZG, Qiu P, Zhou YY, Chen XM, Xie ZX, Xiao Y, et al. 2019. Comparison of combination therapy with methotrexate and sinomenine or leflunomide for active rheumatoid arthritis: a randomized controlled clinical trial. *Phytomedicine*. 57:403–410.
- Jia XY, Chang Y, Sun XJ, Wu HX, Wang C, Xu HM, Zhang L, Zhang LL, Zheng YQ, Song LH, et al. 2014. Total glucosides of paeony inhibit the proliferation of fibroblast-like synoviocytes through the regulation of G proteins in rats with collagen-induced arthritis. *Int Immunopharmacol*. 18(1):1–6.
- Jin S, Hsieh E, Peng L, Yu C, Wang Y, Wu C, Wang Q, Li M, Zeng X. 2018. Incidence of fractures among patients with rheumatoid arthritis: a systematic review and meta-analysis. *Osteoporos Int*. 29(6):1263–1275.
- Kim JH, Jin HM, Kim K, Song I, Youn BU, Matsuo K, Kim N. 2009. The mechanism of osteoclast differentiation induced by IL-1. *J Immunol*. 183(3):1862–1870.
- Komatsu N, Takayanagi H. 2015. Arthritogenic T cells in autoimmune arthritis. *Int J Biochem Cell Biol*. 58:92–96.
- Liu W, Zhang Y, Zhu W, Ma C, Ruan J, Long H, Wang Y. 2018. Sinomenine inhibits the progression of rheumatoid arthritis by regulating the secretion of inflammatory cytokines and monocyte/macrophage subsets. *Front Immunol*. 9:2228.
- McInnes IB, Buckley CD, Isaacs JD. 2016. Cytokines in rheumatoid arthritis – shaping the immunological landscape. *Nat Rev Rheumatol*. 12(1):63–68.
- Nakae S, Nambu A, Sudo K, Iwakura Y. 2003. Suppression of immune induction of collagen-induced arthritis in IL-17-deficient mice. *J Immunol*. 171(11):6173–6177.
- Papadaki M, Rinotis V, Violitzi F, Thireou T, Panayotou G, Samiotaki M, Doumi E. 2019. New insights for RANKL as a proinflammatory modulator in modeled inflammatory arthritis. *Front Immunol*. 10:97–97.
- Qin Y, Zeng HR, Wang L, Ran Q, Peng W, Gao YX, Huang QW, Tan J. 2019. Spectrum-effect relationship between HPLC fingerprint and free radicals scavenging in Guizhi Shaoyao Zhimu Decoction. *Zhongguo Zhong Yao Za Zhi*. 44(14):3042–3048.
- Redlich K, Smolen JS. 2012. Inflammatory bone loss: pathogenesis and therapeutic intervention. *Nat Rev Drug Discov*. 11(3):234–250.
- Scott DL, Wolfe F, Huizinga TW. 2010. Rheumatoid arthritis. *Lancet*. 376(9746):1094–1108.
- Simonet WS, Lacey DL, Dunstan CR, Kelley M, Chang MS, Luthy R, Nguyen HQ, Wooden S, Bennett L, Boone T, et al. 1997. Osteoprotegerin: a novel secreted protein involved in the regulation of bone density. *Cell*. 89(2):309–319.
- Singh JA, Saag KG, Bridges SL Jr, Ak EA, Bannuru RR, Sullivan MC, Vaysbrot E, McNaughton C, Osani M, Shmerling RH, et al. 2016. 2015 American College of Rheumatology Guideline for the treatment of rheumatoid arthritis. *Arthritis Rheumatol*. 68(1):1–26.
- Sinigaglia L, Varenna M, Girasole G, Bianchi G. 2006. Epidemiology of osteoporosis in rheumatic diseases. *Rheum Dis Clin North Am*. 32(4):631–658.
- Smolen JS, Landewe R, Bijlsma J, Burmester G, Chatzidionysiou K, Dougados M, Nam J, Ramiro S, Voshaar M, van Vollenhoven R, et al. 2017. EULAR recommendations for the management of rheumatoid arthritis with synthetic and biological disease-modifying antirheumatic drugs: 2016 update. *Ann Rheum Dis*. 76(6):960–977.
- Sparks JA. 2019. Rheumatoid arthritis. *Ann Intern Med*. 170(1):ITC1–ITC16.
- Tsuboi H, Matsui Y, Hayashida K, Yamane S, Maeda-Tanimura M, Nampei A, Hashimoto J, Suzuki R, Yoshikawa H, Ochi T. 2003. Tartrate resistant

- acid phosphatase (TRAP) positive cells in rheumatoid synovium may induce the destruction of articular cartilage. *Ann Rheum Dis.* 62(3): 196–203.
- Vanderborght A, Linsen L, Thewissen M, Geusens P, Raus J, Stinissen P. 2004. Osteoprotegerin and receptor activator of nuclear factor-kappaB ligand mRNA expression in patients with rheumatoid arthritis and healthy controls. *J Rheumatol.* 31(8):1483–1490.
- Walsh MC, Choi Y. 2014. Biology of the RANKL–RANK–OPG system in immunity, bone, and beyond. *Front Immunol.* 5:511.
- Walsh NC, Gravallese EM. 2010. Bone remodeling in rheumatic disease: a question of balance. *Immunol Rev.* 233(1):301–312.
- Wang M, Huang J, Fan H, He D, Zhao S, Shu Y, Li H, Liu L, Lu S, Xiao C, et al. 2018. Treatment of rheumatoid arthritis using combination of methotrexate and Tripterygium glycosides tablets—a quantitative plasma pharmacokinetic and pseudotargeted metabolomic approach. *Front Pharmacol.* 9:1051.
- Wu M, Wang Y, Deng L, Chen W, Li YP. 2012. TRAF family member-associated NF-κB activator (TANK) induced by RANKL negatively regulates osteoclasts survival and function. *Int J Biol Sci.* 8(10):1398–1407.
- Xiang N, Li XM, Zhang MJ, Zhao DB, Zhu P, Zuo XX, Yang M, Su Y, Li ZG, Chen Z, et al. 2015. Total glucosides of paeony can reduce the hepatotoxicity caused by methotrexate and leflunomide combination treatment of active rheumatoid arthritis. *Int Immunopharmacol.* 28(1): 802–807.
- Xu S, Wang Y, Lu J, Xu J. 2012. Osteoprotegerin and RANKL in the pathogenesis of rheumatoid arthritis-induced osteoporosis. *Rheumatol Int.* 32(11):3397–3403.
- Yang CL, Oi TC, Ho MH, Lau AS. 2013. Scientific basis of botanical medicine as alternative remedies for rheumatoid arthritis. *Clin Rev Allergy Immunol.* 44(3):284–300.
- Zhang Q, Peng W, Wei S, Wei D, Li R, Liu J, Peng L, Yang S, Gao Y, Wu C, et al. 2019. Guizhi-Shaoyao-Zhimu decoction possesses anti-arthritic effects on type II collagen-induced arthritis in rats via suppression of inflammatory reactions, inhibition of invasion & migration and induction of apoptosis in synovial fibroblasts. *Biomed Pharmacother.* 118:109367.